FATIGUE PROPERTY IMPROVEMENT OF TYPE 316L STEEL BY CAVITATION SHOTLESS PEENING

K. MASAKI 1, Y. OCHI 2, H. SOYAMA 3

1 Okinawa National College of Technology, 905 Henoko Nago City
Okinawa 905-2192, Japan
2 University of Electro Communications Tokyo, 1-5-1 Chofugaoka Chofu City
Tokyo 182-8585, Japan
3 Tohoku University, 01 Aoba-yama Aoba-ku Sendai City Miyagi 980-8579, Japan

ABSTRACT
To investigate the effects of cavitation shotless peening (CSP) on the high-cycle fatigue properties of Type 316L austenitic stainless steel, rotating bending fatigue tests were conducted on CSP-treated specimens. The fatigue test results were compared with the fatigue properties of a shot peening (SP) treated specimen rendered under the same fatigue testing conditions. It was found that the high-cycle fatigue properties of Type 316L austenitic stainless steel were improved because CSP treatment induced work hardening of the specimen surface and high compressive residual stress near the surface layers. However, the fatigue property of the CSP-treated specimen did not improve as much as that of the SP-treated specimen. This is attributable to the difference in the amount of plastic deformation near the surface layer induced by the CSP treatment as opposed to the SP treatment.

KEY WORDS
High-cycle fatigue, cavitation shotless peening, austenitic stainless steel, residual stress, fatigue crack behavior

INTRODUCTION
Shot peening (SP) treatment is a very useful method to improve the fatigue property of metal components such as gears and springs. However, SP treatment requires the handing of dust during the treatment and the recovery of shot and disposal of dust afterwards. More recently, some shotless peening techniques that can administer a peening treatment to metals without any shot or grit are attracting attention (Y.Sano et al.,1998; H.Soyama et al.,1998). One such method, cavitation shotless peening (CSP), is an enhanced peening technique using cavitation impact developed by Soyama (H.Soyama et al.,1998). In this process, a cavitation jet is impinged onto a metal surface under water. The collapsing cavitation bubbles cause plastic deformation on the surface, thereby introducing the compressive residual stress.

In the present study, to evaluate the effects of CSP on the high-cycle fatigue properties of Type 316L austenitic stainless steel, rotating bending fatigue tests were carried out. Additionally, comparisons were made between the peening effect of, and resulting fatigue property improvement of, the CSP treatment and those of the SP treatment.

METHODS
The material used in the study was a low-carbon austenitic stainless steel (Type 316L (JIS SUS316L)) that is used in nuclear reactor structures. The chemical

Table 1 Chemical composition of Type 316L [wt%].

C	Si	Mn	P	S	Ni	Cr	Mo
0.017	0.39	0.8	0.029	0.014	12.17	16.31	2.06

composition of the material is shown in Table 1. The material was machined to the shape and the dimensions shown in Figure 1 and was subsequently subjected to full heat treatment in a vacuum (1100°C for 1 h) to homogenize the grains. The central part of the test specimen was then polished with emery paper and buff. This specimen is a non-peened (n.p.) specimen. The microstructure of the material is shown in Figure 2. The mean grain size of the material was approximately 88 μm. After the heat treatment, either CSP treatment or SP treatment was performed. Table 2 lists the CSP treatment conditions, and Table 3, the SP treatment conditions. The specimen was rotated as these peening treatments were performed. Hereafter, the CSP-treated specimen is referred to as the CSP specimen, and the SP-treated specimen, the SP specimen. The SP specimen data are quoted from a past study (K.Masaki et al.,1997).

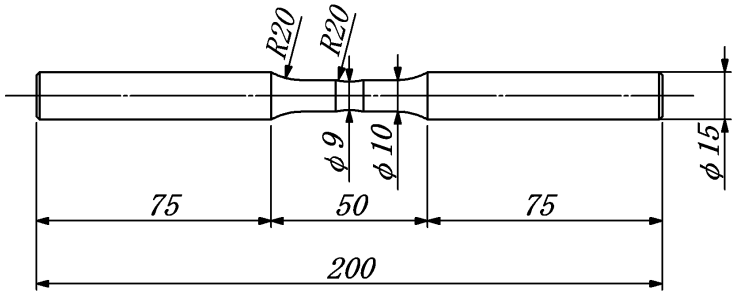

Figure 1 Shape and dimension of fatigue specimens.

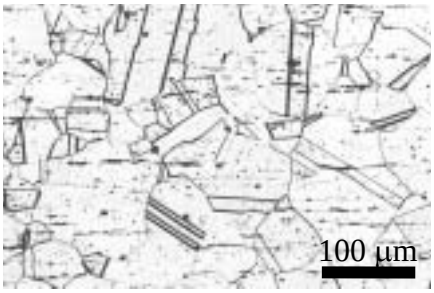

Figure 2 Microstructure of material.

Table 2 Cavitation shotless peening conditions.

Upstream pressure	Processing time	Nozzle diameter	Standoff distance
MPa	s/mm	mm	mm
30	100	1.8	55

Table 3 Shot peening conditions.

Shot grid			Air pressure	Work time	Distance	Almen intensity	Coverage
Material	Size	Hardness					
steel (RCW)	0.3mmϕ	700Hv	0.294MPa	30sec	120mm	0.2mmA	over 100%

High-cycle rotating bending loading fatigue tests with a frequency of 2820 rpm were carried out using circulating distilled water to prevent heating. The fracture surface was observed by scanning electron microscopy (SEM) to examine the fracture mechanism after fatigue fracture, and surface crack propagation was observed by the replication technique.

RESULTS

Peening effect of CSP treatment

Table 4 compares the surface roughness values of the CSP and the SP specimens. Both the center line average values (R_a) and the maximum height of roughness profiles values (R_y) of the CSP specimen are smaller than those of the SP specimen. This slight deterioration in surface roughness is characteristic of CSP treatment.

Figure 3 shows the Vickers hardness at different depths in the specimen. It is found that the thickness of the hardened layer of the CSP specimen is the same as that of the SP specimen: 150 μm. The maximum hardness just under the surface of the CSP specimen is approximately 200 Hv, indicating that the CSP treatment increased the hardness by approximately 40 Hv. However, the maximum hardness of the CSP specimen is approximately 100 Hv lower than the maximum hardness of the SP specimen, which is approximately 300 Hv.

Figure 4 shows the distribution of longitudinal (σ_z) residual stresses at various depths in each of the specimens; these distributions were approximately equal. The compressive residual stress layer was approximately 200–300 μm from the surface of both specimens. Although the maximum residual stress occurred at the surfaces of both, the maximum stress values were approximately −500 MPa for the CSP specimen and −650 MPa for the SP specimen.

Fatigue test results

Figure 5 shows S-N curves for all the specimens. The fatigue strength of the CSP specimen at 10^8 cycles was 240 MPa, which was approximately 1.3 times that of the

Table 4 Surface roughness values

Specimens	R_a μm	R_y μm
n.p.	0.03	0.32
CSP	1.31	7.33
SP	2.2	16

R_a : Center line average
R_y : Maximum height of roughness profiles

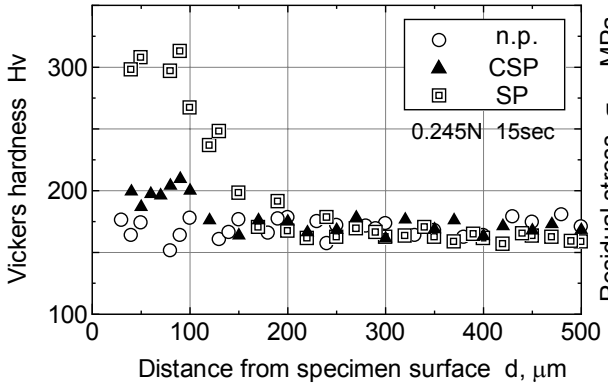

Figure 3 Vickers hardness distributions.

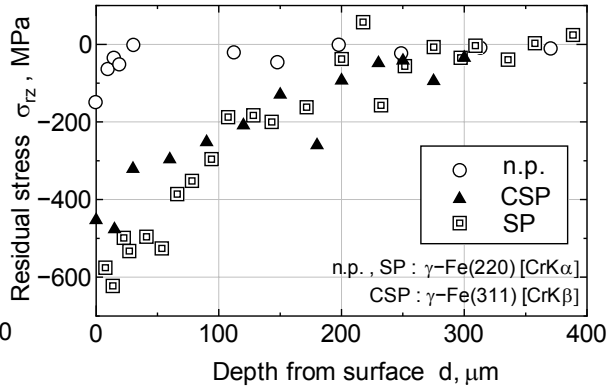

Figure 4 Residual stress distributions.

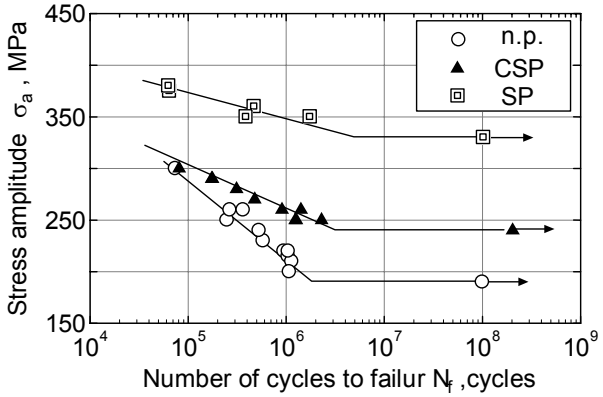

Figure 5 Fatigue results.

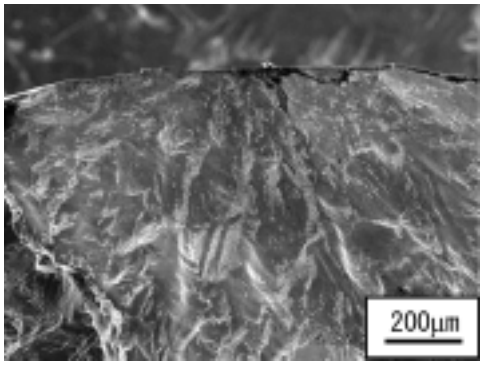

(b) n.p. specimen
(σ_a=240MPa, N_f=5.3x10^5cycles)

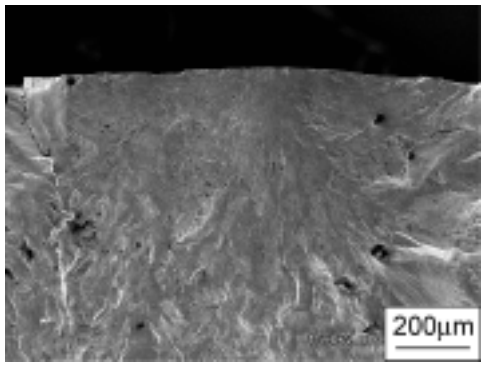

(b) CSP specimen
(σ_a=290MPa, N_f=1.7x10^5cycles)

Figure 6 Example of fracture surface observation results.

n.p. specimen. In comparison, the fatigue strength of the SP specimen at 10^8 cycles was 340 MPa. Figure 6 shows examples of fracture surface observation results by SEM. The fracture surface of the n.p. and CSP specimens show similar surface fracture behavior.

DISCUSSIONS

Comparison between the n.p. and the CSP specimens

From the fatigue results, it is clear that the CSP treatment resulted in an improvement in the fatigue strength of Type 316L austenitic stainless steel. Also, the fatigue life of the CSP specimen was longer than that of the n.p. specimen, exhibited in Figure 5 by the greater stress amplitude required for the CSP specimen to fail at 10^8 cycles compared to that required for the n.p. specimen to fail at the same number of cycles. This is despite the fact that a stress amplitude of 300 MPa was sufficient for failure in both specimens at approximately 10^5 cycles.

To investigate the extension of fatigue life by CSP treatment, surface fatigue crack propagation behavior was investigated using the replication technique at a stress amplitude of 260 MPa. Figure 7 shows the crack propagation curves of the n.p. and CSP specimens. The fatigue crack initiation life of the CSP specimen is longer, and also, the initial crack length of the CSP specimen was smaller than that of the n.p. specimen. In both the CSP and the n.p. specimens, there were a large number of fatigue crack initiations. Figure 8 shows the relationships between crack propagation rate and half-crack length. The data for the CSP specimen shows an extraordinary deceleration in crack propagation rate when the half-crack length is less than 30–50 μm, although both approximately straight lines seem to almost correspond. It is believed that the cause of this deceleration in the crack propagation rate of the CSP

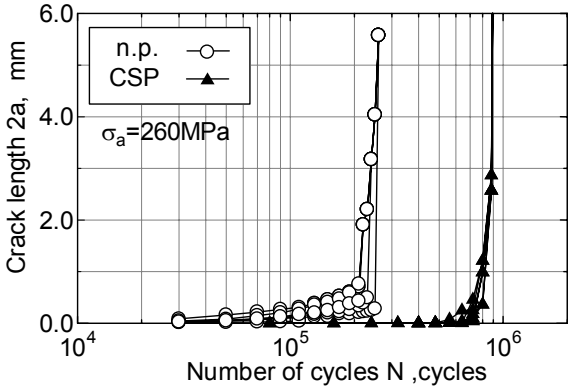

Figure 7 Surface crack propagation curves.

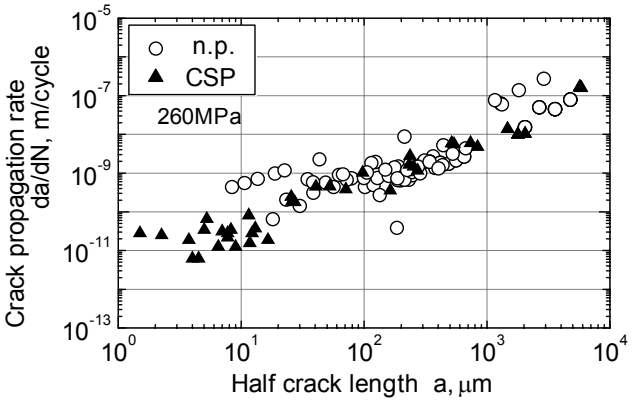

Figure 8 Surface crack propagation rate.

specimen is due to the influence of compressive residual stress. Extension of the fatigue crack initiation life and deceleration of small fatigue crack growth is the cause of the fatigue life extension of the CSP specimen.

Comparison between the CSP and the SP specimens

There was a large difference in fatigue strength between the CSP and the SP specimens. CSP and SP treatments are processes that plastically deform the surfaces of the materials; they can improve the fatigue properties by inducing work hardening and compressive residual stress. One of the reasons for this difference in fatigue strength improvement is the difference in the amount of the plastic deformation induced; therefore, in this study, the estimation of plastic strain on the surfaces of the CSP and the SP specimens was performed.

Figure 9 shows the relationships between the Vickers hardness and pre-plastic strain of tensile-deformed Type 316L austenitic stainless steel. From this, it can be predicted that the plastic strains of the SP and CSP specimens are approximately 40% and 5%, respectively, because the Vickers hardness values of the matrices at a 50 μm depth in the SP and the CSP specimens are approximately 300 Hv and 200 Hv, respectively, as shown in Figure 3.

Figure 10 shows the relationships between the tensile strength and pre-plastic strain of pre-strained Type 316L. The 0.2% proof strength of the work-hardened section at the surface of the CSP specimen is approximately 300 MPa because the plastic strain is approximately 5%. This 0.2% proof strength almost corresponds to the absolute value of the compressive residual stress at a 50 μm depth in the CSP specimen. This correspondence suggests that the residual stress resulting from CSP

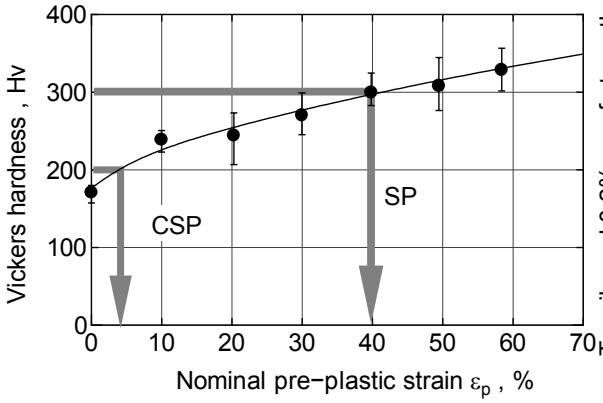

Figure 9 Vickers hardness of plastic-strained Type316L.

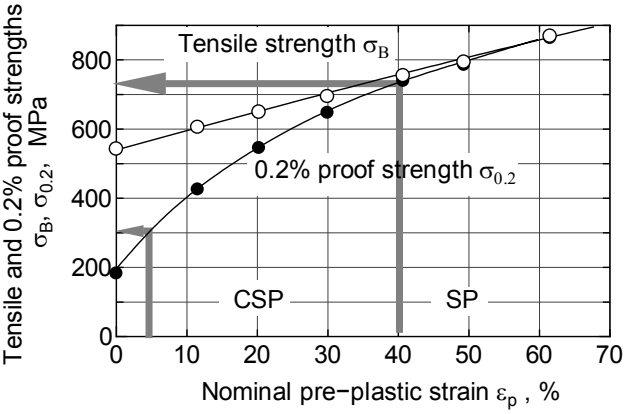

Figure 10 Tensile strength of plastic-strained Type316L.

treatment is plastic deformation, even though CSP treatment is not a surface hardening treatment that causes much of a plastic deformation. The 0.2% proof strength of the SP specimen, however, is approximately 750 MPa, because the value of its plastic deformation, approximately 40%, is higher than the absolute value of the compressive residual stress of the SP specimen. It seems that this is due to the fact that structural refinement is caused by the remarkably high plastic strain at the specimen surface resulting from the SP treatment.

CONCLUSIONS

The high-cycle fatigue property was improved by CSP treatment. And comparing the fatigue properties of the CSP specimen with those of a conventional SP specimen showed the following:

(1)The fatigue strength at 10^8 cycles was improved by approximately 50 MPa by the CSP treatment under the conditions used in this study.

(2)The surface roughness value of the CSP specimen was smaller than that of the SP specimen.

(3)The thickness of the surface-hardened layer in the CSP specimen was approximately 150 μm, and the maximum Vickers hardness value was approximately 200 Hv. Although the thickness of the CSP specimen was almost the same as that of the SP specimen, the maximum value for the CSP specimen was approximately 100 Hv lower than that of the SP specimen.

(4)The trend of the plot of residual stress distribution for the CSP specimen was the same as that for the SP specimen. However, the maximum residual stress value of the CSP specimen was approximately 200 MPa lower than that of the SP specimen.

(5)A large number of small fatigue cracks of 10 μm or less in half-crack length were initiated at an early fatigue stage. These fatigue cracks grow slowly, and most of the fatigue life was spent by the time the crack length reaches approximately 100 μm.

REFERENCES

K. Masaki, Y. Ochi and A. Ishii, J. Soc. Mat. Sci. Japan, Vol.46, No.10, pp.1130–1135,
(1997)

Y. Sano, M. Yoda, N. Mukai and M. Obata, Laser Review, Vol.26, No.11, pp.793–799, (1998)

H. Soyama, J.D. Park, M. Saka and H. Abe, J. Soc. Mat. Sci. Japan, Vol.47, No.8, pp.808–812 (1998)